

## Enhanced Photothermal Methane Dry Reforming through Electronic Interactions between Nickel and Yttrium

Xueying Zhang <sup>a,b,c</sup>, Zeshu Zhang <sup>a,b,c,\*</sup>, Qishun Wang <sup>c,d</sup>, Jianheng Xu <sup>a,b,c</sup>, Xinyu Han <sup>a,b,c</sup>, Jiakun Wang <sup>a,b,c</sup>, Jia Liu <sup>a,b,c</sup>, Cheng Rao, <sup>a,b,c</sup> Yibo Zhang <sup>a,b,c,\*</sup>, Xiangguang Yang <sup>a,b,c</sup>, Lu Wang <sup>e,\*</sup>

<sup>a</sup> School of Rare Earths, University of Science and Technology of China, Hefei 230026, China

<sup>b</sup> Ganjiang Innovation Academy, Chinese Academy of Sciences, No.1, Science Academy Road, Ganzhou 341000, China

<sup>c</sup> Key Laboratory of Rare Earths, Chinese Academy of Sciences, Ganzhou 341000, China

<sup>d</sup> Changchun Institute of Applied Chemistry, Chinese Academy of Sciences, Changchun, 130022, China

<sup>e</sup> School of Science and Engineering, The Chinese University of Hong Kong, Shenzhen, 518172 Shenzhen, Guangdong, China.

\* E-mail addresses (Corresponding authors):

zszhang@gia.cas.cn (Zeshu Zhang); yibo Zhang@gia.cas.cn (Yibo Zhang); lwang@cuhk.edu.cn (Lu Wang)

### **Preparation of reagent**

Without further purification, the following chemical reagents were used: Urea ( $\geq 99.5\%$ , Aladdin), deionized water (self-made), hexadecyl trimethyl ammonium bromide (CTAB, Aladdin), cyclohexane (AR, Macklin), 1-Hexanol (99%, Macklin), tetraethyl orthosilicate (TEOS, GC,  $>99\%$ , Macklin), anhydrous ethanol ( $\geq 99.0\%$ , Shanghai Hushi),  $\text{Ni}(\text{NO}_3)_2 \cdot 6\text{H}_2\text{O}$  (AR 98%, Xilong Science). Ethylene glycol (AR,  $\geq 99.5\%$ , Xilong Science),  $\text{Y}(\text{NO}_3)_3 \cdot 6\text{H}_2\text{O}$  (99.99% metals basis, Aladdin),  $\text{SiO}_2$  (99.99%, Macklin).

## The conversion rate of CO<sub>2</sub>

The conversion rate of CO<sub>2</sub> is calculated by Equation (S1):<sup>1</sup>

$$X_{CO_2} = \frac{F_{in.CO_2} - F_{out.CO_2}}{F_{in.CO_2}} * \% \quad (S1)$$

Where,  $X_{CO_2}$  represents the conversion rate of CO<sub>2</sub>, %.  $F_{in.CO_2}$  represents the amount of CO<sub>2</sub> before the reaction, %.  $F_{out.CO_2}$  represents the amount of CO<sub>2</sub> after the reaction, %.

## **Details of DFT calculation**

To explore the light adsorption ability of catalysts at the molecular level, we conducted density functional theory (DFT) calculations to analyze the differential charge density and density of states. All computations were performed using the CASTEP module within Materials Studio 2020. The generalized gradient approximation (GGA) combined with the Revised Perdew-Burke-Ernzerhof (RPBE) functional was utilized for geometry optimization and energy evaluations of the catalyst. Norm-conserving pseudopotentials were specified for these computations.

Before geometry optimization, the parameters were set as follows. LBFGS method was used as the algorithm. And we also adjusted the convergence tolerance. The energy was set as  $2.0 \times 10^{-5}$  eV/atom. The cell optimization option was set as none for all models. The parameters in the electronic options were also customized. The energy cut-off was set as 800 eV and the SCF tolerance was set as  $1.0 \times 10^{-6}$  eV/atom. For density mixing, the charge is 0.5 and the spin is 2.0. The K-point set was  $1 \times 1 \times 1$  for all models.

For the geometry optimization of the NiY/KCC-1 catalyst, the spin polarization option was set as collinear, and the spin magnetic moment was set as 3. DFT+U method was used and the values were 2.0 eV and 2.5 eV for the 3d orbital of Y and Ni.

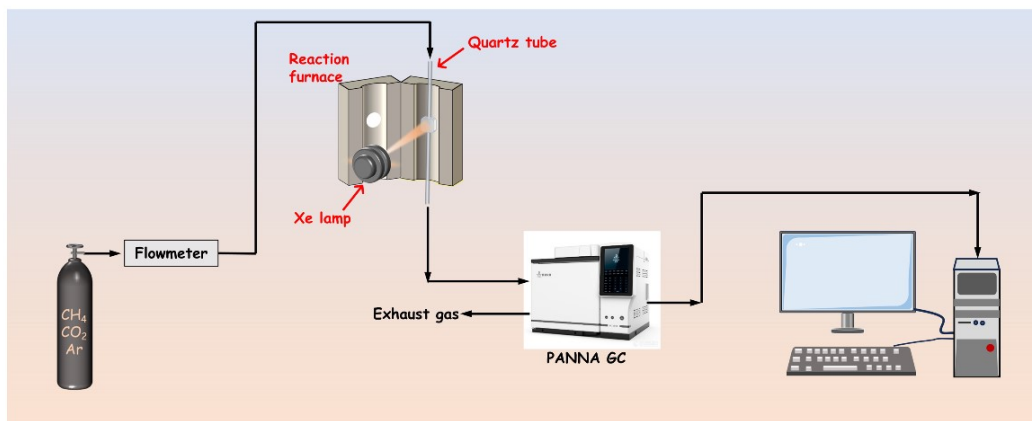


Fig. S1. Schematic of the photothermal reaction system.

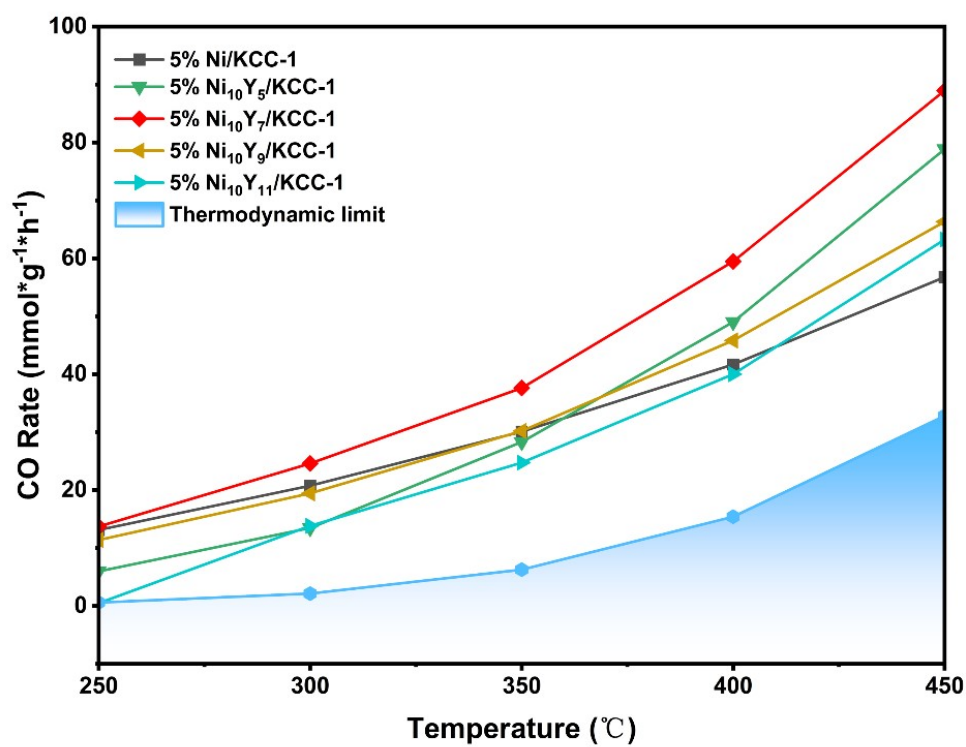


Fig. S2. CO formation rate over the samples with different Y-doping amounts under light.

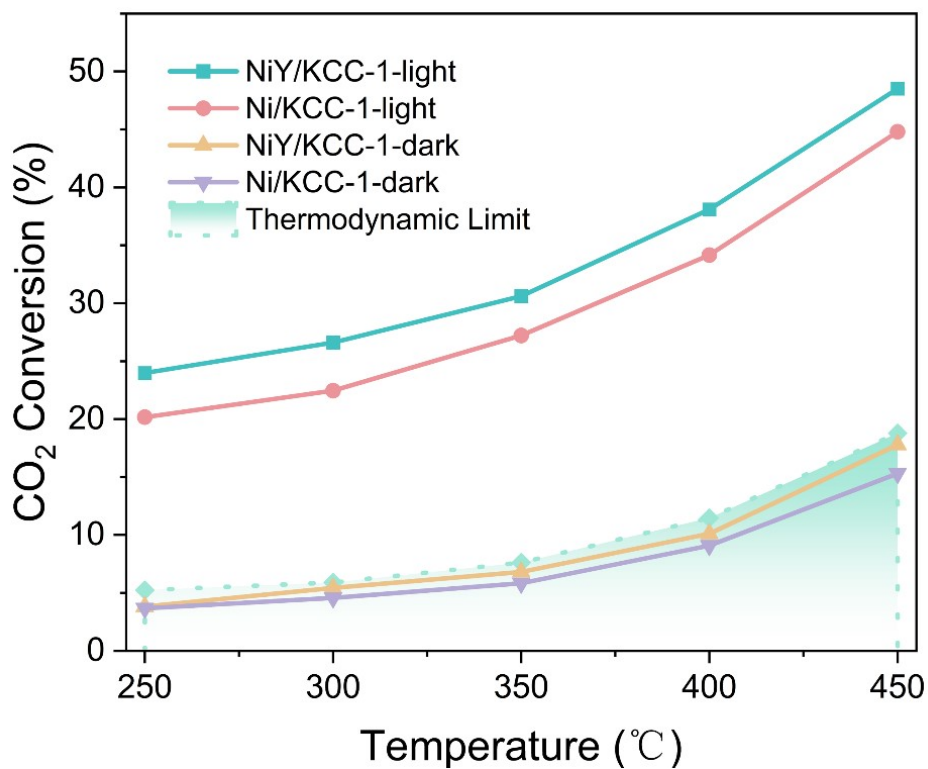


Fig. S3. CO<sub>2</sub> conversion of NiY series catalysts at different temperatures

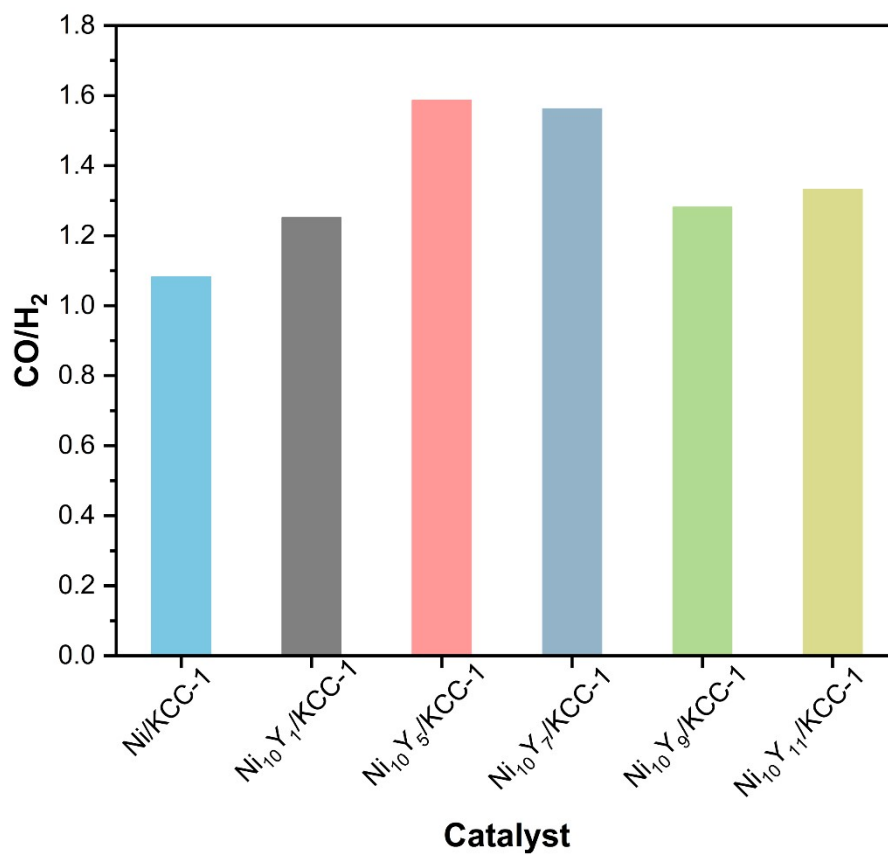
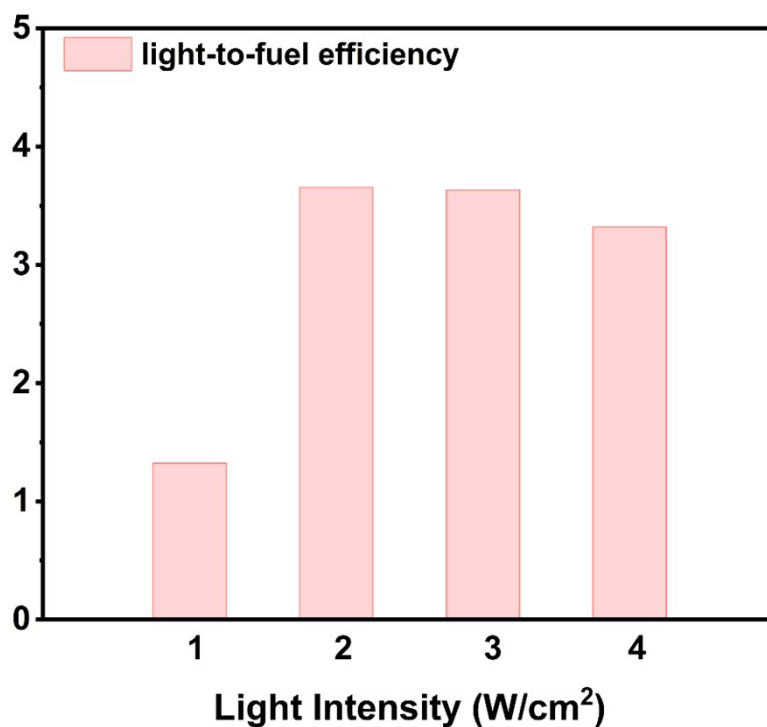
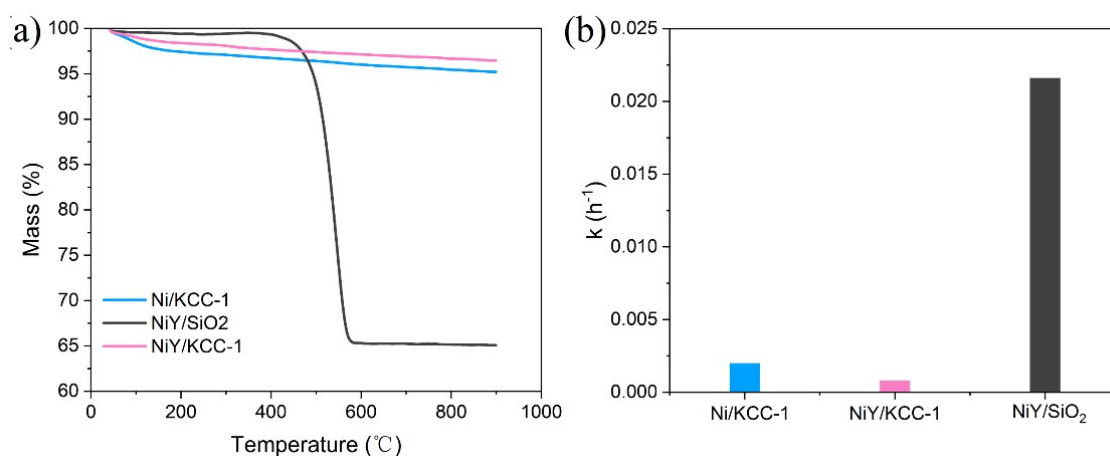


Fig. S4. CO/H<sub>2</sub> of different samples at 450°C under light conditions.



**Fig. S5.** The light-to-fuel efficiency of NiY/KCC-1 at different light intensities.



**Fig. S6.** (a) TGA profiles and (b) Carbon deposition rate of the used Ni/KCC-1, NiY/KCC-1, and NiY/SiO<sub>2</sub> after photothermal stability tests.

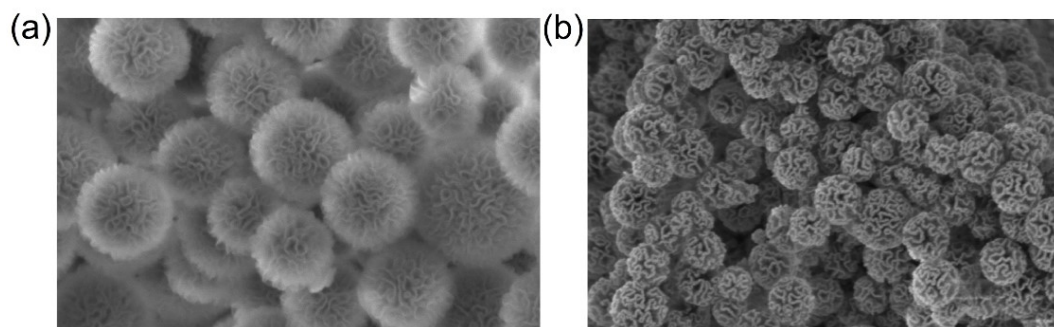


**Fig. S7.** The SEM images of (a) KCC-1 and (b) NiY/KCC-1.

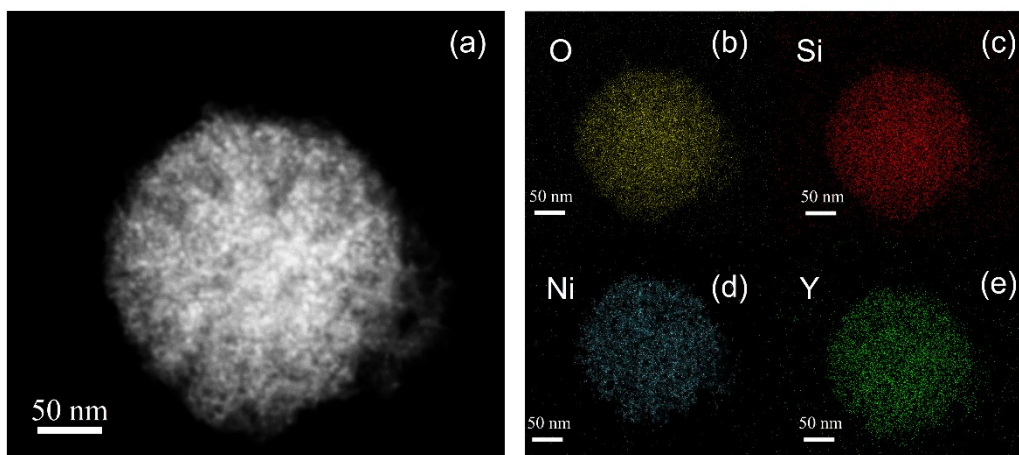


**Fig. S8.** (a)-(e) EDS mappings (O element-g, Si element-j, Ni element-i, Y element-k) of NiY/KCC-1.

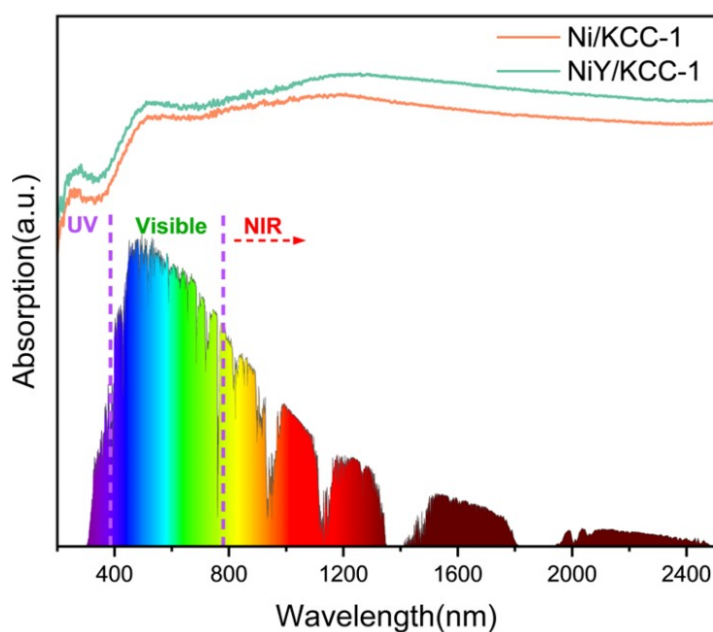


**Fig. S9.** UV vis absorbances of Ni/KCC-1 and NiY/KCC-1.

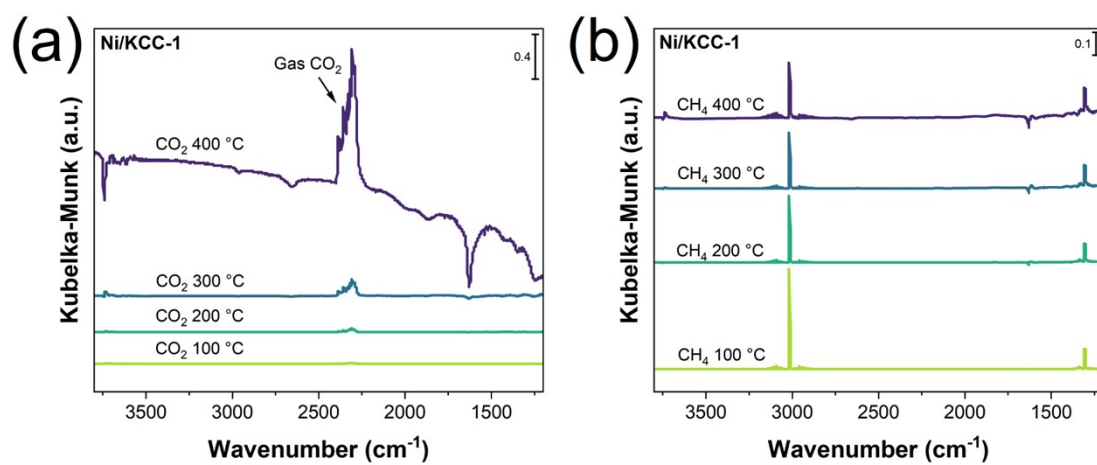


**Fig. S10.** In situ DRIFT spectra of the adsorption of (a)  $\text{CO}_2$  and (b)  $\text{CH}_4$  at different temperatures of Ni/KCC-1 under light.

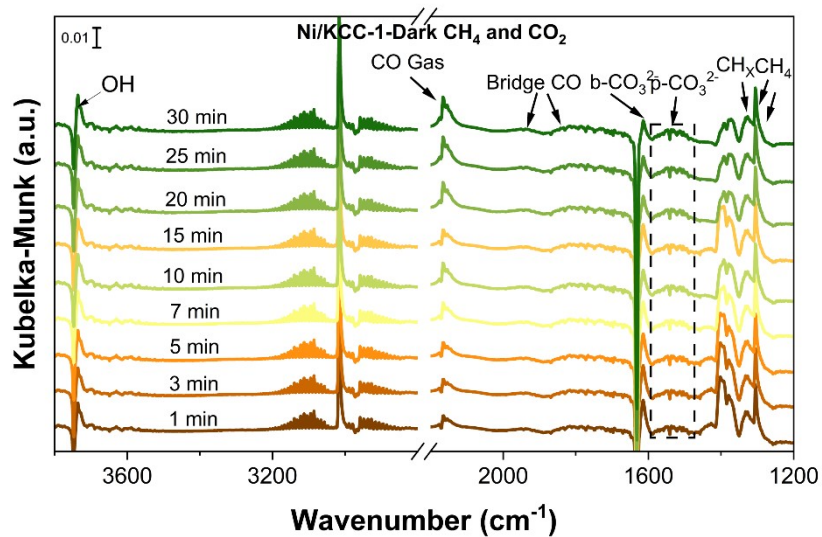


**Fig. S11.** In situ DRIFT spectra of the reaction of  $\text{CH}_4$  and  $\text{CO}_2$  at different times of Ni/KCC-1 in the dark.

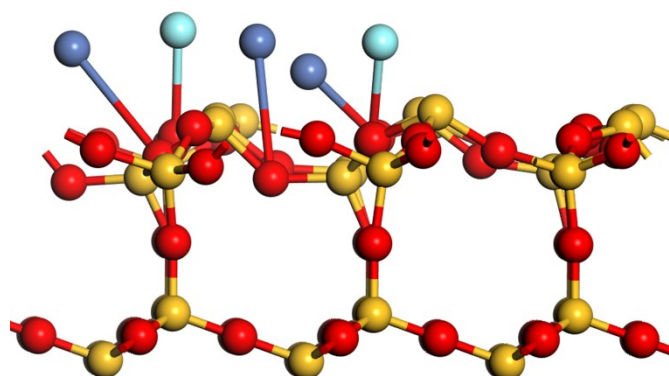


**Fig. S12.** The NiY/KCC-1 model of side views is used for the calculation.

## Notes and references

1. X. Zhao, S. Sun, Y. Wang, Y. Zhang, Y. Zhu, B. Zong, J. Hu, P. Williams and C. Wu, *Chemical Engineering Journal*, 2024, **491**.